

Supermassive black hole feedback quenches disc galaxies and suppresses bar formation in TNG50

Matthew Frosst^{1,2*}, Danail Obreschcow^{1,2}, Aaron Ludlow^{1,2}, Connor Bottrell¹, and Shy Genel^{3,4}

¹International Centre for Radio Astronomy Research (ICRAR), University of Western Australia, Crawley, WA 6009, Australia

²ARC Centre of Excellence for All Sky Astrophysics in 3 Dimensions (ASTRO 3D)

³Center for Computational Astrophysics, Flatiron Institute, 162 5th Avenue, New York, NY 10010, USA

⁴Columbia Astrophysics Laboratory, Columbia University, 550 West 120th Street, New York, NY 10027, USA

Accepted XXX. Received YYY; in original form ZZZ

ABSTRACT

We use the cosmological magneto-hydrodynamical simulation TNG50 to study the relationship between black hole feedback, the presence of stellar bars, and star formation quenching in Milky Way-like disc galaxies. Of our sample of 198 discs, about 63 per cent develop stellar bars that last until $z = 0$. After the formation of their bars, the majority of these galaxies develop persistent 3–15 kpc wide holes in the centres of their gas discs. Tracking their evolution from $z = 4$ to 0, we demonstrate that barred galaxies tend to form within dark matter haloes that become centrally disc dominated early on (and are thus unstable to bar formation) whereas unbarred galaxies do not; barred galaxies also host central black holes that grow more rapidly than those of unbarred galaxies. As a result, most barred galaxies eventually experience kinetic wind feedback that operates when the mass of the central supermassive black hole exceeds $M_{\text{BH}} \gtrsim 10^8 M_{\odot}$. This feedback ejects gas from the central disc into the circumgalactic medium and rapidly quenches barred galaxies of their central star formation. If kinetic black hole feedback occurs in an unbarred disc it suppresses subsequent star formation and inhibits its growth, stabilising the disc against future bar formation. Consequently, most barred galaxies develop black hole-driven gas holes, though a gas hole alone does not guarantee the presence of a stellar bar. This subtle relationship between black hole feedback, cold gas disc morphology, and stellar bars may provide constraints on subgrid physics models for supermassive black hole feedback.

Key words: galaxies: evolution – galaxies: kinematics and dynamics – galaxies: bar

1 INTRODUCTION

In the Λ CDM cosmology, the dark matter density field of the universe is nearly scale-free, but the galaxies embedded within it are not. One of the most significant transitions in galaxy properties occurs near the mass of the Milky Way (MW), corresponding to a halo mass of $\sim 10^{12} M_{\odot}$. At this scale, the galaxy population gradually transitions from star-forming discs to quiescent spheroids (e.g. Moffett et al. 2016). Intriguingly, even within the disc population substantial changes occur around this mass scale. For example, more massive galaxies become increasingly bulge-dominated (Bell et al. 2017), the incidence of stellar bars may increase (Melvin et al. 2014; Gavazzi et al. 2015; Erwin 2018), and cold gas deficits that reduce star formation (SF) activity become more common (e.g. Kauffmann et al. 2003). Moreover, massive discs interact more strongly with their central supermassive black holes (SMBHs), which become increasingly active, as demonstrated by the rising fraction of Seyfert galaxies above this mass scale (Sampaio et al. 2023).

While the observational evidence for these transitions is robust, the underlying mechanisms that cause them remain under debate. Specifically, the relationships between bars, SMBH feedback, and the quenching of SF are not yet fully understood. Accreting SMBHs

require gas to be transported to the disc centre as fuel, with torques from bars being a possible driver (Maciejewski 2004; Jøgee 2006; Fanali et al. 2015). However, bar driven SMBH fueling remains controversial: some observations suggest that SMBH activity is enhanced by the presence of a bar (Knapen et al. 2000; Laine et al. 2002; Silva-Lima et al. 2022; Garland et al. 2024), while others do not (Lee et al. 2012; Goulding et al. 2017; Zee et al. 2023).

From a theoretical standpoint, simulating the interplay between stellar bars, SMBHs, and SF is difficult to study because it demands high-resolution simulations that incorporate uncertain sub-grid models to capture complex physics below the resolution limit. Simulations provided the first compelling evidence that SMBH feedback plays a crucial role in quenching the population of massive galaxies (e.g. Springel et al. 2005; Bower et al. 2006; Dubois et al. 2013; Weinberger et al. 2018). More recently, simulations have been used to quantify the importance of SMBH feedback on the properties of gas in galaxies (e.g., Davies et al. 2020; Zinger et al. 2020; Ramesh et al. 2023; Wellons et al. 2023), and to constrain SMBH models (e.g. Genel et al. 2014). However, despite significant effort, the mechanisms by which energy from SMBH feedback couples to the gas, as well as the importance of other heating mechanisms, are not yet understood (e.g. McNamara & Nulsen 2007; Yuan & Narayan 2014).

Stellar bars are ubiquitous among galaxies in the local universe (Masters et al. 2011), and are thus frequently studied using cosmolog-

* E-mail: matt.frosst@icrar.org

ical simulations (e.g. Blázquez-Calero et al. 2020; Ansar et al. 2023; Fragkoudi et al. 2024). Simulated barred galaxies tend to be gas poor and quenched, as expected (Algorry et al. 2017; Rosas-Guevara et al. 2020, 2022; Zhu et al. 2020). Furthermore, Zana et al. (2019) showed that SMBH feedback can influence the properties of bars, for example causing them to be shorter and weaker than they otherwise would be (see also Irodotou et al. 2022; Zhou et al. 2020; Semczuk et al. 2024), though the interactions between bars and SMBHs remain unclear.

However, robustly simulating the formation of stellar bars in disc galaxies is not trivial. Although it is not difficult to produce bars in simulations of disc-dominated systems (Hohl 1971; Ostriker & Peebles 1973; Athanassoula & Sellwood 1986), the challenge lies in generating populations of barred galaxies with converged quantitative properties, such as their incidence, formation time, length, and pattern speed. For instance, convergence studies using idealised simulations show that including live dark matter haloes that can interact with the bar is crucial, and that simulations require $\sim 10^6$ disc particles and $\sim 10^7$ dark matter halo particles to achieve reliable results (e.g. Dubinski et al. 2009; Frosst et al. 2024). These requirements challenge cosmological hydrodynamical simulations, which typically produce galaxies with far fewer stellar and dark matter particles.

The aim of this study is to explore the connection between SMBH feedback, stellar bars, and SF quenching in disc galaxies using a state-of-the-art cosmological simulation from the IllustrisTNG project (hereafter TNG). Specifically, we focus on a carefully selected and well-studied sample of 198 MW- and M31-like disc galaxies from TNG50 (see Pillepich et al. 2023). This sample allows us to simultaneously focus on the mass scale where the aforementioned scale-dependent features of disc galaxies become significant and to reach the high resolutions required to reliably model bars properties. Additionally, this disc sample consists of galaxies in isolated environments (at $z = 0$), enabling us to focus primarily on the internal processes driving secular bar formation.

This paper is organised as follows. In Section 2, we describe the TNG50 simulation and the disc sample that we use for our analysis; we then introduce various definitions and analysis techniques. In Section 3 we present the results of our analysis and explain the links between SMBH feedback, central gas disc morphology, and the formation of stellar bars. Finally, we summarise our results in Section 4.

2 METHODS

For our analysis, we adopt a cylindrical coordinate system whose z -axis is aligned with the total angular momentum vector of stellar particles and star-forming gas cells within two stellar half mass radii, $r_{\star,1/2}$. In this coordinate system, $r = (R^2 + z^2)^{1/2}$ is the 3D radial coordinate, where $R = (x^2 + y^2)^{1/2}$ is the distance from the z -axis, and z is the height above the disc.

2.1 The TNG50 simulation

We focus on the TNG50 simulation (TNG50-1; Pillepich et al. 2019; Nelson et al. 2019a,b), which is the highest resolution simulation of the TNG project (Marinacci et al. 2018; Naiman et al. 2018; Nelson et al. 2018; Springel et al. 2018; Pillepich et al. 2018a; Nelson et al. 2019a). The simulation was run with the AREPO moving-mesh code (Springel 2010), using cosmological parameters from Planck Collaboration et al. (2016).

TNG50 follows the evolution of gas cells, dark matter (DM), black

hole and stellar particles, and magnetic fields from $z = 127$ to $z = 0$ in a 51.7 cMpc volume (note that length units prefixed with a "c" are co-moving). The simulation initially has 2×2160^3 mass elements, half of which are DM particles with mass $4.5 \times 10^5 M_{\odot}$ and the other half are gas cells with a target mass of $8.5 \times 10^4 M_{\odot}$. The Plummer equivalent gravitational softening length of gas elements is dynamically adapted to the effective cell radius, but has a minimum value of $\epsilon_g = 72$ pc. Collisionless particles (DM and stars) have a Plummer softening length of $\epsilon_c = 575$ cpc until $z = 1$, below which they have a fixed physical softening length of $\epsilon_c = 288$ pc.

TNG50 includes models for star formation, stellar feedback, active galactic nuclei (AGN) feedback, supermassive black hole growth, stellar evolution, and chemical enrichment (see Pillepich et al. 2018b; Springel et al. 2018; Nelson et al. 2018; Naiman et al. 2018; Marinacci et al. 2018, for details). Details about the subgrid physics and calibration process can be found in Weinberger et al. (2017) and Pillepich et al. (2018a).

Galaxies and DM haloes were identified using the SUBFIND algorithm (Springel et al. 2001) and linked between snapshots by the SUBLINK merger tree code (Rodríguez-Gomez et al. 2015). SUBFIND also returns a number of basic properties of haloes, for instance, M_{200c} , the mass within the radius r_{200c} that encloses a mean density equal to 200 times the critical density of the universe.

2.2 The TNG50 MW/M31-like sample

We focus our analysis on the sample of MW/M31 analogs in TNG50 curated by Pillepich et al. (2023). This sample fulfills the following criteria at $z = 0$:

- (i) The stellar mass, M_{\star} (measured within $r \leq 30$ kpc), is in the range $10^{10.5} M_{\odot} < M_{\star} \leq 10^{11.2} M_{\odot}$, and the host halo mass is $M_{200c} < 10^{13} M_{\odot}$;
- (ii) The stellar disc has a minor-to-major axis ratio $c/a \leq 0.45$ (measured between $1 - 2 r_{\star,1/2}$) or it appears visually disc-like with obvious spiral arms, and;
- (iii) No other galaxies with $M_{\star} \geq 10^{10.5} M_{\odot}$ are within 500 kpc.

A total of 198 disc galaxies satisfy these criteria. More details about their selection can be found in Pillepich et al. (2023).

2.3 The implementation of SMBH in TNG

The SMBH model used for TNG is described in Weinberger et al. (2017). In brief, SMBHs are seeded with an initial mass of $M_{\text{BH}} = 1.18 \times 10^6 M_{\odot}$ in haloes whose friend-of-friends mass (Davis et al. 1985) exceeds $\geq 7.38 \times 10^{10} M_{\odot}$, provided they do not already contain one. SMBHs can grow through mergers or by accreting mass from neighbouring gas cells at the Eddington-limited Bondi accretion rate:

$$\dot{M}_{\text{BH}} = \min(\dot{M}_{\text{bondi}}, \dot{M}_{\text{edd}}), \quad (1)$$

where

$$\dot{M}_{\text{bondi}} = \frac{4\pi G^2 M_{\text{BH}}^2 \rho_g}{c_s^3} \quad (2)$$

and

$$\dot{M}_{\text{edd}} = \frac{4\pi G M_{\text{BH}} m_p}{\sigma_{\text{T}} \epsilon_r c} \quad (3)$$

are the Bondi-Hoyle–Lyttleton (Hoyle & Lyttleton 1939; Bondi & Hoyle 1944; Bondi 1952) and Eddington accretion rates, respectively. Here, G is the gravitational constant, c is the vacuum speed of light,

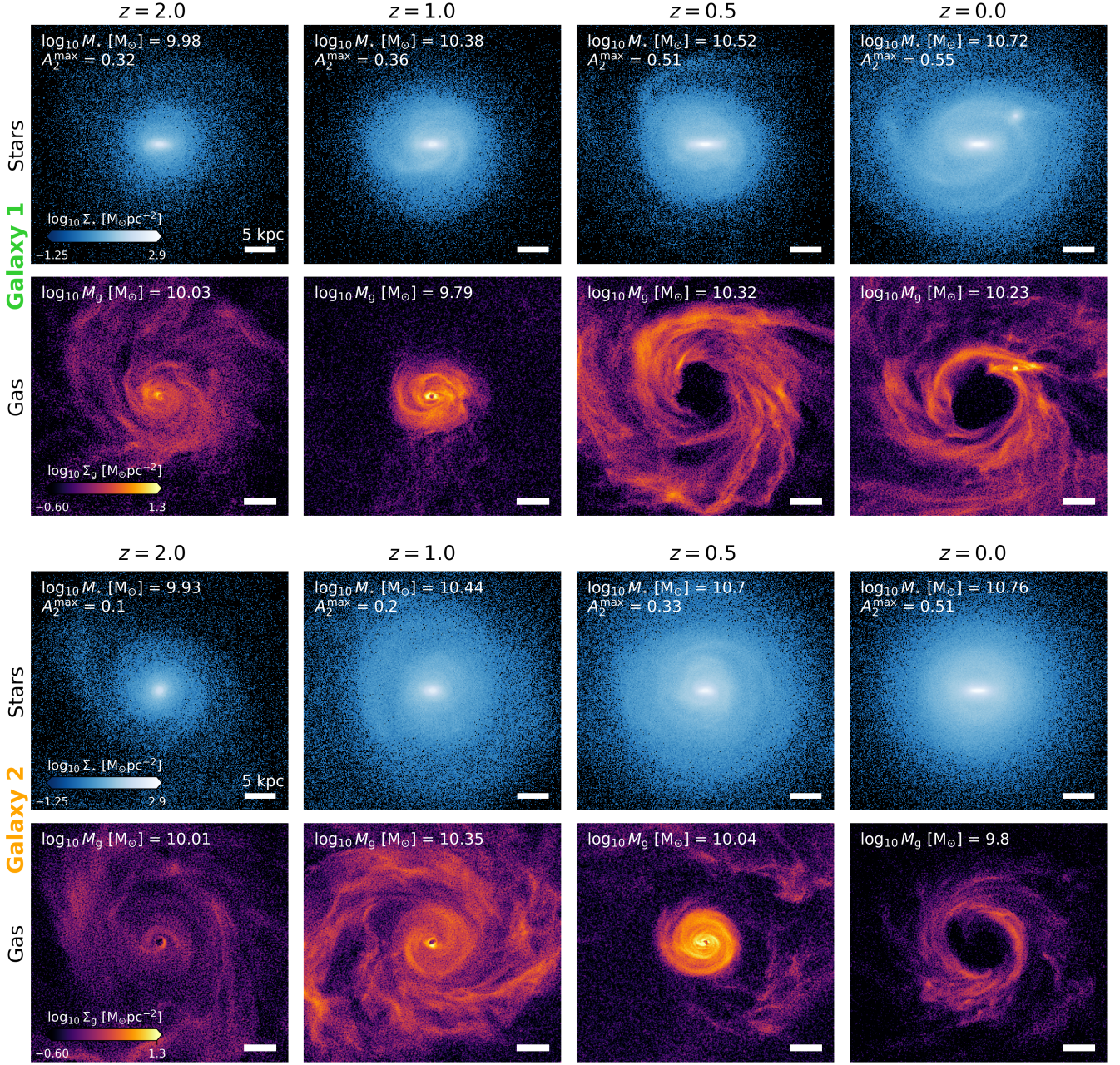


Figure 1. The different panels show snapshots of the time evolution from $z = 2$ to 0 (left to right) of two example galaxies: subfindID 530852 (Galaxy 1) is shown in the upper two rows, and subfindID 534628 (Galaxy 2) in the lower two rows. For each galaxy, we show the face-on stellar surface mass density (Σ_* ; top rows, blue colours) and gas surface mass density (Σ_g ; bottom rows, red colours). In the top left corner of the Σ_* panels we label the stellar mass within $r \leq 30$ kpc and bar strength. Similarly, in the top left corner of the Σ_g panels we label the gas mass within $r \leq 30$ kpc. The white lines in the bottom right of each panel have a length of 5 kpc.

σ_T is the Thompson cross-section, and m_p is the proton mass. The parameter $\epsilon_r = 0.2$ is the radiative accretion efficiency, and ρ_g and c_s are the average density and sound speed of the neighbouring 646 gas cells.

Some of the energy accreted is released back into the surrounding gas cells as feedback. In TNG, there are two modes of SMBH feedback: (1) at high accretion rates, it is injected as pure thermal energy (hereafter “thermal mode” feedback), and (2) at low accretion rates, it is injected as momentum kicks (hereafter “kinetic mode”). The mode

of SMBH feedback depends on whether the Bondi-Hoyle-Lyttleton accretion rate exceeds a M_{BH} -dependent fraction of the Eddington accretion rate: SMBH feedback is in kinetic mode when

$$\chi = \frac{\dot{M}_{\text{bondi}}}{\dot{M}_{\text{eddi}}} < \chi_{\text{thresh}} \equiv \min \left(0.002 \left(\frac{M_{\text{BH}}}{10^8 M_{\odot}} \right)^2, 0.1 \right), \quad (4)$$

and is in thermal mode otherwise. We define the lookback time at which the central SMBH first enters kinetic feedback mode as t_{kin} , i.e. the time of the first snapshot at which $\chi < \chi_{\text{thresh}}$.

2.4 Characterising stellar bars in TNG50

We characterize stellar bars using a Fourier decomposition of the face-on stellar surface mass density (Athanasoula & Misiriotis 2002; Dehnen et al. 2023; Frosst et al. 2024). The strength (A_m) and phase angle (ϕ_m) of a bar is related to the amplitude of the even Fourier modes; they are calculated as follows:

$$A_m = |\mathcal{A}_m| \quad (5)$$

and

$$\phi_m = \frac{1}{m} \arg(\mathcal{A}_m), \quad (6)$$

where

$$\mathcal{A}_m = \frac{\sum_j M_j e^{mi\theta_j}}{\sum_j M_j}. \quad (7)$$

In the latter, M_j and θ_j are the mass and azimuthal angle of the j^{th} stellar particle, and m is the order of the Fourier mode. We measure the lowest order bar strength profile, $A_2(R)$, in radial bins. The bar strength, A_2^{max} , is defined as the maximum value of $A_2(R)$ and has a phase angle defined as ϕ_2^{max} . The bar length, R_{bar} , is identified as the maximum extent beyond A_2^{max} where $\phi_2(R)$ deviates from ϕ_2^{max} by $\leq \pm 10^\circ$ while $A_2(R) \geq A_2^{\text{max}}/2$, following the procedure described in Dehnen et al. (2023). We follow Rosas-Guevara et al. (2022), and define barred galaxies as those with both $A_2^{\text{max}} > 0.2$ and $R_{\text{bar}} \geq 1.4\epsilon_c$, ensuring a constant $\phi_2(R)$ in the galaxy centre before bars are identified. The bar formation time, t_{bar} , is defined as the first time a galaxy is barred and remains so for at least three consecutive snapshots (≈ 450 Myr).

All galaxies are visually inspected at each snapshot to ensure our measurements are not corrupted by transient events like mergers. At $z = 0$, 125 of the galaxies in our sample have stellar bars, roughly 63 per cent, in good agreement with observations of galaxies in the local universe and with other studies based on TNG50 (e.g. Sheth et al. 2008; Nair & Abraham 2010; Masters et al. 2011; Gargiulo et al. 2022; Rosas-Guevara et al. 2022).

3 LINKS BETWEEN QUENCHING, SMBHS, AND BARS

3.1 A case study of two barred galaxies

To set the stage, in Fig. 1 we plot the stellar and gas face-on surface mass densities for two example galaxies at $z = 2, 1, 0.5$, and 0 (left to right, respectively). By $z = 0$, both galaxies have developed prominent holes in their central gas distributions. These holes effectively halt star formation, leaving the inner 3 kpc largely or entirely quenched: the $z = 0$ star formation rates (SFRs) within $r = 3$ kpc are $0 M_\odot \text{yr}^{-1}$ and $10^{-3.9} M_\odot \text{yr}^{-1}$ for Galaxy 1 and 2¹, respectively (SFRs below $10^{-2.5} M_\odot \text{yr}^{-1}$ are considered unresolved and are hence equivalent to no SF, see Donnari et al. 2019). By $z = 0$, both galaxies host stellar bars, clearly visible in their stellar surface mass density distributions ($A_2^{\text{max}} = 0.55$ and 0.51 for Galaxy 1 and 2, respectively), and also have central SMBHs operating in kinetic feedback mode.

Both the kinetic feedback and bar dynamics could, a priori, contribute to the central quenching of SF. For instance, bars may stabilize gas discs against SF (but leave inert gas in the galaxy centre, e.g. Khoperskov et al. 2018), or gas influenced by the bar may trigger nuclear SF and BH accretion, ultimately stifling the central SF once

¹ Galaxies 1 and 2 have SubfindIDs 530852 and 534628 at $z = 0$, respectively

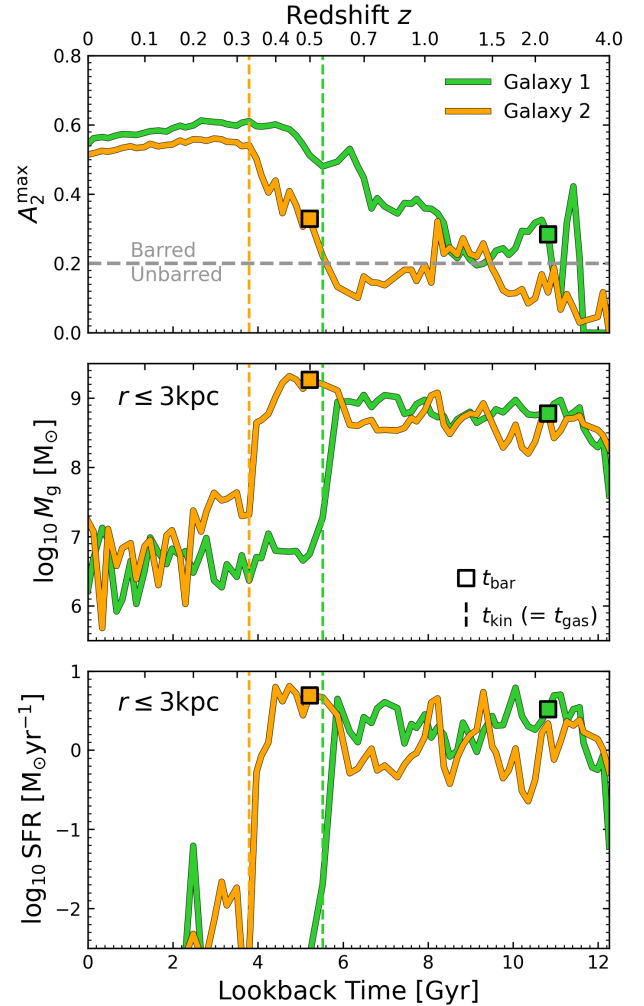


Figure 2. The bar strength, A_2^{max} (upper panel), the central gas mass, M_g ($r \leq 3$ kpc) (middle panel), and the central SFR within the same radius (lower panel), as a function of time from $z = 4$ to 0. We plot the evolutionary histories of the two example galaxies from Fig. 1, Galaxy 1 and Galaxy 2, as green and orange lines, respectively. The bar formation time, t_{bar} , is plotted as a coloured square for each galaxy. The gas hole formation time, t_{gas} , and the time at which the central SMBH first enters kinetic feedback mode, t_{kin} , occur at the same time and are plotted as coloured vertical dashed lines.

the gas is consumed (e.g. Fanali et al. 2015). On the other hand, for reasons unrelated to the bar, SMBH kinetic feedback may eject gas from the galaxy centre, removing the fuel for SF (e.g. Davies et al. 2020; Terrazas et al. 2020). The clue to distinguishing these mechanisms lies in the evolutionary histories of these galaxies.

In Fig. 2 we show the time evolution of the stellar bar strength, A_2^{max} (upper panel), the total gas mass within 3 kpc of each galaxy's centre (middle panel), and the SFR within the same radius (lower panel) for the two example galaxies. The evolution of A_2^{max} shows that both galaxies host long-lived bars that persist to $z = 0$; the values of t_{bar} are marked along each of the curves using squares. Immediately after their bars form, the central gas mass and SFR of each galaxy is largely unchanged: this is particularly evident for Galaxy 1, whose central gas fraction and SFR remains approximately constant for ≈ 5 Gyr following t_{bar} . Eventually, however, both galaxies experience sudden drop ($\approx 1 - 2$ dex) in their central gas mass and SFR, which

lasts to $z = 0$; this corresponds to the formation of the gas holes already apparent in Fig. 1. We mark this drop with a vertical dashed line, and denote it t_{gas} . Hereafter, t_{gas} is defined as the time at which the gas-to-stellar mass ratio (within 3 kpc) drops below 1 per cent and remains so for at least three consecutive snapshots (≈ 450 Myr); as seen in the bottom panel of Fig. 2, t_{gas} coincides with star formation quenching.

By analyzing the trajectories of tracer particles, we verified that immediately after t_{gas} the vast majority of the central gas mass is ejected into the circumgalactic medium of the galaxies, rather than being consumed by star formation (see Genel et al. 2013, for details). This suggests that feedback from SMBHs leads to the formation of the central gas holes. Indeed, t_{kin} , i.e. the first snapshot at which the central SMBH is in kinetic mode, exactly coincides with t_{gas} at the time resolution of the simulation and also occurs at the time marked by the vertical dashed lines in Fig. 2. Evidently, both of these galaxies form stellar bars before their gas holes develop, but their gas holes are first identified in the same snapshot that the SMBH enters kinetic feedback mode.

3.2 Black hole feedback quenches star formation in barred galaxies

In Fig. 3 we show that the results from the case study in Section 3.1 apply to the whole sample. The dashed blue and solid black lines show, respectively, the cumulative fraction of all galaxies that have formed gas holes by a particular time (i.e. the distribution of t_{gas}) and those that have entered kinetic feedback mode (i.e. the distribution of t_{kin}); they are essentially indistinguishable. This indicates that the formation of holes in the central gas distribution of discs coincide with the SMBH entering kinetic feedback mode (we have verified this for each galaxy individually). Only about 6 per cent of galaxies with gas holes have $t_{\text{kin}} \neq t_{\text{gas}}$. We conclude that gas holes form as a result of SMBH kinetic feedback (in agreement with Li et al. 2020; Terrazas et al. 2020; Zinger et al. 2020; Pillepich et al. 2021), and are not caused by stellar bars.

Note also that the majority of galaxies that host stellar bars develop gas holes after their bars form. The solid red line in Fig. 3 shows the distribution of t_{bar} (i.e. the cumulative fraction of all galaxies that have formed a stellar bar by time t , and that remain barred until $z = 0$). Contrast this with the short-dashed red line, which shows the cumulative fraction of the same barred galaxies that have formed gas holes. Although these distributions differ, they reveal that about 92 per cent of all barred galaxies eventually develop central gas holes, and that bars almost always form first. Conversely, only around 8 per cent of barred discs in our sample do not have holes in their central gas distributions at $z = 0$. This is a non-trivial result that we return to in Section 3.3.

Given that $t_{\text{gas}} \approx t_{\text{kin}}$ for almost all of the discs, it is clear that gas holes form due to kinetic winds from the central SMBH, rather than through a bar driven process. We confirm this in Fig. 4, where we plot the $z = 0$ Bondi-to-Eddington accretion rate ratio, χ , versus M_{BH} . Discs are split into barred and unbarred (red and blue points, respectively), and galaxies with and without gas holes (open and closed circles, respectively). For comparison, the grey points show all other SMBHs in TNG50 (no distinction has been made between centrals and satellites), and coloured lines show the trajectories of Galaxy 1 and 2 from Fig. 1. The separation between galaxies whose SMBH are in thermal versus kinetic feedback mode is shown as a dashed grey line (defined by eq. 4 in Section 2.3).

Fig. 4 elicits some comments. First, two distinct black hole populations are evident: those in thermal feedback mode (high χ ,

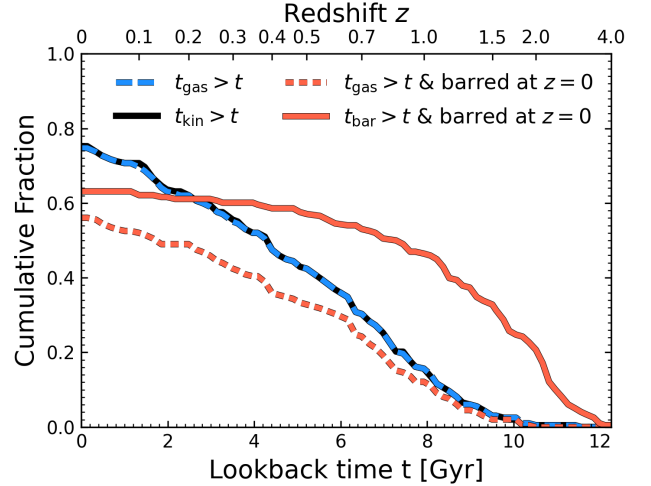


Figure 3. The dashed blue and solid black lines show, respectively, the cumulative fractions of galaxies that have developed gas holes (i.e. the distribution of t_{gas}) and those that have central SMBHs in kinetic feedback mode (i.e. the distribution of t_{kin}). The solid and dashed red lines show, respectively, the fraction of all galaxies that have developed persistent stellar bars (i.e. the distribution of t_{bar} for discs that host stellar bars at $z = 0$) and the subset of barred galaxies that have formed gas holes. Gas holes almost always appear in the same snapshot in which SMBH kinetic feedback is initiated. About 90 per cent of all barred galaxies eventually develop gas holes (but some galaxies with gas holes at $z = 0$ are not barred).

$M_{\text{BH}} \lesssim 10^8 M_{\odot}$), and those in kinetic feedback mode (low χ , $M_{\text{BH}} \gtrsim 10^8 M_{\odot}$). Second, all galaxies with holes in the centres of their gas discs at $z = 0$ have SMBHs operating in kinetic feedback mode (i.e., the open circles are below the grey dashed line), and most, but not all, of these galaxies are barred (about 77 per cent of discs in kinetic mode at $z = 0$ are barred; red open circles). This clearly shows that the gas holes (and subsequent quenching) are driven by SMBH kinetic winds rather than bar driven quenching. Similar gas holes have been found in other galaxy formation simulations that employ two-mode SMBH feedback (e.g. Irodoto et al. 2022; Wellons et al. 2023; Arora et al. 2024). However, this does not explain why most discs in our sample that contain central gas holes are also barred.

The green and orange lines in Fig. 4 show that the example galaxies above initially host low-mass SMBHs operating in thermal feedback mode. As their central SMBHs grow, they later enter kinetic mode feedback when $M_{\text{BH}} \gtrsim 10^8 M_{\odot}$. Furthermore, the early bar formation in Galaxy 1 (green line) does not significantly affect the evolutionary history of its SMBH during the nearly 5 Gyr between t_{bar} and t_{kin} . When $t_{\text{bar}} \gg t_{\text{kin}}$ (green line), the SMBH has relatively low mass at t_{bar} and is operating in thermal mode for much of the galaxy’s history, but if $t_{\text{bar}} \approx t_{\text{kin}}$ (orange line), the galaxy forms a bar when the SMBH is already massive and about to enter kinetic feedback mode.

In Fig. 5 we plot the $z = 0$ instantaneous SFR of gas cells versus M_{\star} (both quantities were measured within $r = 30$ kpc). For comparison, we plot the star formation main sequence (SFMS) for TNG50 as a solid grey line (Donnari et al. 2019) and the remaining TNG50 galaxies as grey points. As in Fig. 4, we distinguish barred and unbarred galaxies (red and blue points, respectively) and galaxies with and without gas holes (open and closed circles, respectively). Galaxies with gas holes (which also have SMBH in kinetic feedback mode) have lower SFRs than galaxies without gas holes. This is true

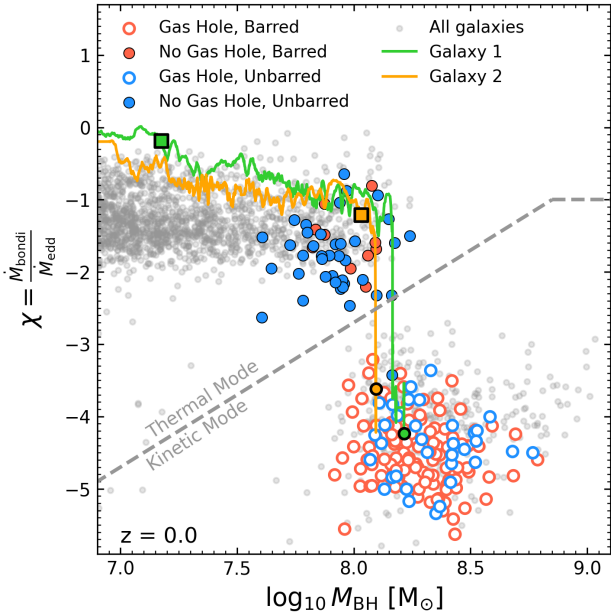


Figure 4. The $z = 0$ Bondi-to-Eddington accretion rate ratio, χ , for central SMBHs plotted as a function of black hole mass, M_{BH} . The critical accretion ratio that determines whether a black hole is in thermal or kinetic feedback mode is plotted as a grey dashed line (defined by Eq. 4). Coloured symbols show the sample of discs used in our study, split into those that are barred and unbarred (red and blue symbols, respectively), and that those that do or do not have central gas holes (open and closed symbols, respectively). All other TNG50 galaxies are shown as grey points for comparison. Trajectories for the two example galaxies in Figs. 1 and 2 are plotted as green and orange lines; squares of corresponding colour indicate t_{bar} for these two systems. Galaxies with gas holes have central black holes that operate exclusively in kinetic feedback mode, and many of them also host stellar bars.

regardless of whether the galaxy is barred or not. For our sample of TNG50 discs, SMBH feedback is an efficient quenching mechanism, whereas stellar bars do not influence the SFR either globally or locally.

3.3 Secular bar formation is halted in galactic discs that have been quenched by black hole feedback

We have established that the gas holes present in many of the discs in our sample are created by kinetic BH feedback and not by stellar bars. Nevertheless, galaxies with prominent gas holes are preferentially barred, and vice versa. We next explore the relation between the presence of stellar bars and gas holes.

In Fig. 6 we plot the lookback times at which galaxies develop their gas holes (t_{gas}) versus the time at which they form their stellar bars (t_{bar}); note that only barred galaxies that also contain gas holes are plotted. This comparison reveals that bars almost always form *before* gas holes do, as expected from Fig. 3. Only eight galaxies form a stellar bar after a gas hole has already formed; visual inspection suggests that most of these eight bars were triggered by a passing satellite galaxy.

To highlight how these timescales relate to SMBH feedback, we shaded the points in Fig. 6 by the mass of the galaxy’s central SMBH at t_{bar} , i.e. by $M_{\text{BH}}(t_{\text{bar}})$. Galaxies with the largest time delay between t_{bar} and t_{gas} also have the lowest-mass SMBHs at t_{bar} (represented by

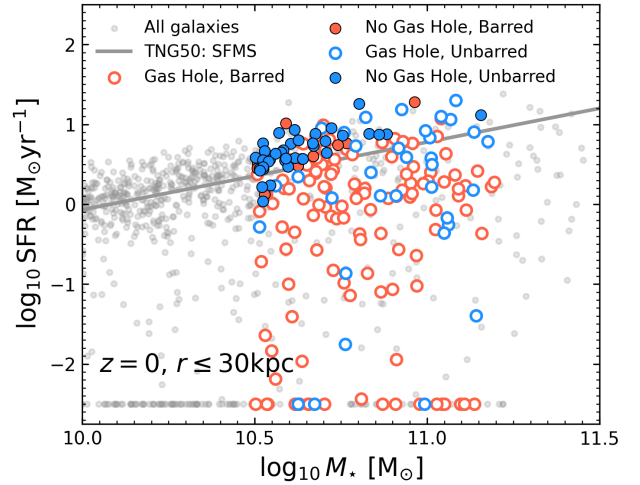


Figure 5. The $z = 0$ SFR plotted versus galaxy stellar mass; both quantities were measured within an aperture of $r = 30$ kpc. Coloured symbols follow the plotting conventions used for Fig. 4. The presence of a gas hole driven by SMBH kinetic feedback clearly affects a galaxy’s star formation rate. Whether a galaxy hosts a bar or not has no effect. For comparison, we plot the star formation main sequence (SFMS) for TNG50 as a solid grey line; grey points show individual galaxies not in our sample. The band of galaxies with $\text{SFR} = 10^{-2.5} \text{ M}_{\odot} \text{ yr}^{-1}$ have unresolved SFRs.

black points) – their bars form long before their SMBHs are massive enough to enter kinetic feedback mode. On the other hand, galaxies with $M_{\text{BH}}(t_{\text{bar}}) \geq 10^8 \text{ M}_{\odot}$ tend to develop central gas holes shortly after their bars form (i.e. the white points have $t_{\text{gas}} \approx t_{\text{bar}}$). This is because, in the TNG model, SMBHs enter kinetic mode when they reach a critical mass $M_{\text{BH}} \gtrsim 10^8 \text{ M}_{\odot}$ (see Fig. 4, and Terrazas et al. 2020; Zinger et al. 2020). But why are galaxies apparently unable to form stellar bars *after* their SMBHs enter kinetic mode?

In the upper panels of Fig. 7 we plot the time evolution of the median stellar-to-dark matter mass ratio (measured within the evolving stellar half-mass radius, $r_{\star,1/2}$) for several subsets of our disc sample. In the lower panel we plot the evolution of the median M_{BH} for the same galaxy samples. The various samples comprise galaxies that have never formed bars, and those that form bars secularly.² Discs that were never barred are plotted using dashed blue lines if they do not possess a gas hole and as solid black lines if they do possess a gas hole. The galaxies that form bars secularly – almost all of which also possess gas holes – were split into three bins of t_{bar} : those in the upper quartile of t_{bar} (red lines), those in the lower quartile of t_{bar} (light pink lines), and those in between. Along each of these curves, we plot the median values of t_{bar} , t_{gas} , and t_{kin} as squares, upward triangles, and downward triangles, respectively.

The curves plotted in the upper panel of Fig. 7 show the median stellar-to-dark matter mass ratio (within $r_{\star,1/2}$) of barred discs exceeds that of unbarred discs at all times. Note too that barred galaxies

² Galaxies that host secular bars are those that have not experienced a merger with a stellar mass ratio $\mu \geq 0.1$ within 500 Myr of t_{bar} (see Bottrell et al. 2024, for details about how these mergers are defined). Importantly, we determine μ by evaluating it at the snapshot at which the mass of the least massive progenitor is the greatest (e.g. Soitto-Ramos et al. 2022). Using merger time windows that are reasonably larger or smaller than 500 Myr does not affect our results.

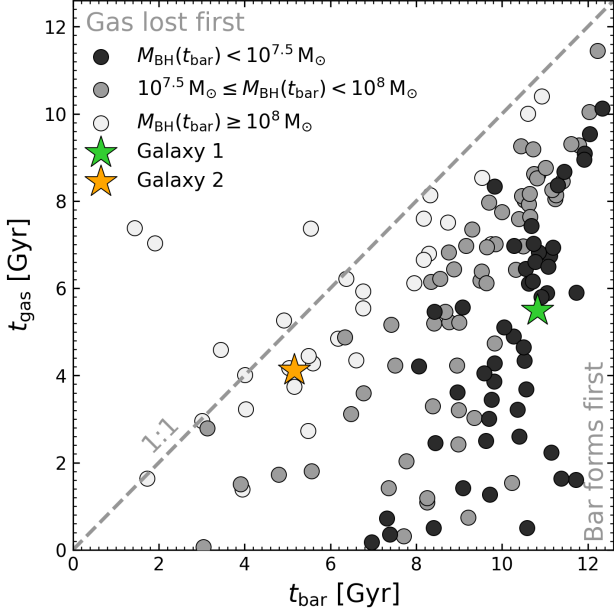


Figure 6. The lookback time at which gas holes form, t_{gas} , plotted versus the bar formation time, t_{bar} . Points are shaded according to $M_{\text{BH}}(t_{\text{bar}})$, i.e. the mass of the central SMBH at t_{bar} . The two example galaxies from Fig. 1 are shown as green and orange stars, as labeled. Note that for the vast majority of galaxies $t_{\text{bar}} \geq t_{\text{gas}}$, and that the relation between them differs depending on the mass of the central black hole at t_{bar} : galaxies with $M_{\text{BH}}(t_{\text{bar}}) \approx 10^8 M_{\odot}$ (the critical mass for kinetic BH feedback; see Fig. 4) have $t_{\text{gas}} \approx t_{\text{bar}}$, whereas those with $M_{\text{BH}}(t_{\text{bar}}) < 10^{7.5} M_{\odot}$ have $t_{\text{gas}} \ll t_{\text{bar}}$. Galaxies in our sample rarely develop stellar bars after t_{gas} .

become disc dominated ($M_{\star}/M_{\text{h}} > 1$) before their bars form, and those that form their bars earlier also become disc dominated earlier (see also Kraljic et al. 2012; Sheth et al. 2012). In contrast, galaxies that never form bars are dark matter-dominated within their stellar half-mass radii at all times. Having a gravitationally-dominant disc appears to be a prerequisite for bar formation (see also Rosas-Guevara et al. 2020; López et al. 2024; Fragkoudi et al. 2024). This agrees with the early analytic work of Ostriker & Peebles (1973), who showed that strongly self-gravitating discs are susceptible to bar formation.

The lower panel of Fig. 7 shows that galaxies that become disc dominated and form secular bars earlier also tend to have central SMBH that grow more rapidly at early times (see also Rosas-Guevara et al. 2020; Zhou et al. 2020). These early growing SMBHs eventually reach sufficiently high masses ($M_{\text{BH}} \gtrsim 10^8 M_{\odot}$) to drive kinetic winds that quench their galaxies, but this usually occurs after the galaxies have already become disc-dominated and therefore susceptible to bar formation. This is the case for the barred galaxy samples represented by red lines in Fig. 7; the downward triangles along these lines mark t_{kin} , which occurs long after $M_{\star}/M_{\text{h}} > 1$.

However, for a small number of galaxies, the SMBHs will grow sufficiently massive to drive kinetic winds and quench the galaxy *before* the disc’s gravity dominates that of the halo. These galaxies (represented by the black lines in Fig. 7) do not form bars because the disc was unable to become sufficiently massive to enable bar formation before being quenched: at early times, these galaxies have similar stellar-to-dark matter mass fractions to those hosting late-forming secular bars (light pink line), but after kinetic feedback is triggered by a period of exceptionally fast black hole growth, their stellar-to-dark

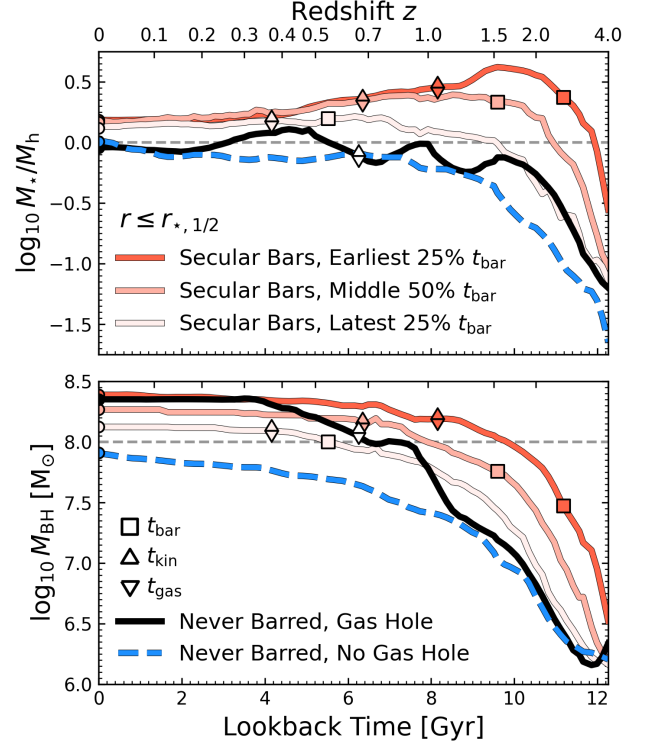


Figure 7. The median stellar-to-dark matter mass ratio (measured within $r_{\star,1/2}$; upper panel) and median SMBH mass (lower panel) as a function of lookback time. Lines with a red hue correspond to galaxies that form stellar bars secularly; they are divided into separate bins based on the relative time at which their bars formed (as indicated in the legend). The blue dashed line corresponds to the sample of galaxies that never formed bars, and the black line shows galaxies that never formed bars but did form gas holes. The horizontal grey dashed line in the upper panel separates galaxies that are disc-dominated ($M_{\star}/M_{\text{h}} \geq 1$) and dark matter-dominated ($M_{\star}/M_{\text{h}} < 1$). In the lower panel, the horizontal grey dashed line correspond to $M_{\text{BH}} = 10^8 M_{\odot}$, roughly the critical mass for kinetic SMBH feedback. Note that disc galaxies will only develop stellar bars after they become disc-dominated, and they only develop gas holes provided $M_{\text{BH}} \gtrsim 10^8 M_{\odot}$.

matter mass ratios level off and they remain dark matter-dominated thereafter. Indeed, for all galaxies in our sample, M_{\star}/M_{h} remains constant or declines after they are subject to strong SMBHs feedback. On the other hand, the late forming galaxies represented by the blue dashed line do not have bars – because they were never disc dominated – or gas holes – because M_{BH} never crossed the critical threshold for kinetic feedback. The high fraction of barred galaxies with gas holes and the fact that gas holes tend to form after stellar bars both have their origins in the co-evolution of the stellar disc mass and the mass of the central SMBH.

4 SUMMARY AND CONCLUSIONS

We used 198 isolated disc galaxies from TNG50 that span the mass range $10^{10.5} \leq M_{\star}/M_{\odot} \leq 10^{11.2}$ (see Pillepich et al. 2023, for details) to study the connection between supermassive black hole feedback, star formation quenching, the morphology of gas discs, and the formation of stellar bars. Our main conclusions are as follows:

- (i) By $z = 0$, many (63 per cent) of the galaxies in our sample have

developed bars in their stellar discs and/or 3 – 15 kpc wide "holes" in their gas discs (75 per cent). The formation of central gas holes quenches the central star formation rates (Fig. 2). Intriguingly, almost all barred galaxies possess gas holes, and in almost every case the bar forms prior to the formation of the gas hole (Fig. 3). At first glance, this seems to imply that bars may be responsible for the formation of gas holes and the subsequent quenching of star formation, as is occasionally suggested by observations (e.g. Masters et al. 2011; George et al. 2019; Fraser-McKelvie et al. 2020; Newnham et al. 2020).

(ii) However, in Section 3.2 we showed that almost all galaxies whose centers are gas poor have also been subject to strong kinetic feedback from their central supermassive black holes (SMBHs), and that the gas holes appear immediately after the SMBHs enter kinetic feedback mode (see Fig. 3), occurring when the SMBH mass exceeds $M_{\text{BH}} \gtrsim 10^8 M_{\odot}$ (Fig. 4). This suggests that, for TNG50, kinetic winds from SMBHs are sufficiently strong to eject gas from the centres of discs, overpowering any stellar bar-driven quenching processes (Fig. 5). Support for this conclusion is provided by a subset of galaxies (roughly 17 per cent of the total sample) whose stellar discs are not barred but whose gaseous discs have nonetheless developed central holes as soon as the SMBHs turn to kinetic feedback.

(iii) Galaxies whose SMBHs enter kinetic feedback mode are largely quenched of star formation thereafter (Fig. 5). This explains why the formation of stellar bars always precedes the formation of gas holes (Fig. 6): if galaxies are not massive enough to support the growth of bar instabilities before being quenched by SMBH feedback, their stellar discs will remain gravitationally subdominant thereafter, and thus stable to bar formation (Fig. 7). Exceptions to this (i.e. when bars form after gas holes) appear possible, for example when bars are triggered at externally through tidal encounters with passing satellite galaxies. We plan to address the latter point in future work using a larger sample of disc galaxies that are not subject to the strong isolation criterion imposed on the sample studied here.

(iv) The high fraction of barred galaxies with gas holes has its origin in the co-evolution of the stellar disc mass and the mass of the central SMBH. Galaxies that form massive discs at early times also form massive BHs at early times, and are thus susceptible to both secular bar formation – which occurs when the stellar mass exceeds the dark matter mass within $r_{\star,1/2}$ – and to kinetic SMBH feedback (Fig. 7).

An important implication of our study is that fine-tuned models for SMBH feedback can have significant effects on the properties of stellar bars (such as their ages, and the galaxies in which they are able to form) and on the inner morphology and star formation rates of gas discs. A note of caution, however, is that our analysis focused on a set of isolated disc galaxies that span a relatively narrow range of halo masses ($10^{11.5} \lesssim M_{200c}/M_{\odot} \lesssim 10^{12.8}$), which is roughly where SMBH feedback and bar formation are common. Our analysis was also based on only one simulation, TNG50, for which kinetic BH feedback is particularly efficient at quenching galaxies (e.g. Terrazas et al. 2020). Future work should extend our analysis to a broader range of galaxy masses and environments, using hydrodynamical simulations that employ different models for SMBH feedback. While real HI gas holes are observed in some galaxies (e.g. George et al. 2019; Newnham et al. 2020; Murugesan et al. 2019), this does not mean that all of the gas is removed or subject to phase change. Careful comparison of the incidence of stellar bars and the morphology of gas discs found in simulations and in observations can possibly be used to constrain subgrid models for SMBH feedback.

ACKNOWLEDGEMENTS

We thank Lars Hernquist and Amelia Fraser-McKelvie for useful conversations. ADL and DO acknowledge financial support from the Australian Research Council through their Future Fellowship scheme (project numbers FT160100250, FT190100083, respectively). CB gratefully acknowledges support from the Forrest Research Foundation. This research was undertaken with the assistance of resources and services from the National Computational Infrastructure (NCI), which is supported by the Australian Government. The IllustrisTNG simulations were undertaken with compute time awarded by the Gauss Centre for Supercomputing (GCS) under GCS Large-Scale Projects GCS-ILLU and GCS-DWAR on the GCS share of the supercomputer Hazel Hen at the High Performance Computing Center Stuttgart (HLRS), as well as on the machines of the Max Planck Computing and Data Facility (MPCDF) in Garching, Germany. This work has benefited from the following public PYTHON packages: SCIPY (Virtanen et al. 2020), NUMPY (Harris et al. 2020), and MATPLOTLIB (Hunter 2007).

DATA AVAILABILITY

The TNG50 simulation data (and MW/M31-like sample) are publicly available; see Nelson et al. (2019a), Pillepich et al. (2018a), and Pillepich et al. (2023) for further information. Additional data can be made available upon reasonable request.

REFERENCES

- Algorry D. G., et al., 2017, *MNRAS*, 469, 1054
- Ansar S., Pearson S., Sanderson R. E., Arora A., Hopkins P. F., Wetzel A., Cunningham E. C., Quinn J., 2023, *arXiv e-prints*, p. [arXiv:2309.16811](https://arxiv.org/abs/2309.16811)
- Arora N., Courteau S., Macciò A. V., Cho C., Patel R., Stone C., 2024, *MNRAS*, 529, 2047
- Athanassoula E., Misiriotis A., 2002, *MNRAS*, 330, 35
- Athanassoula E., Sellwood J. A., 1986, *MNRAS*, 221, 213
- Bell E. F., Monachesi A., Harmsen B., de Jong R. S., Bailin J., Radburn-Smith D. J., D’Souza R., Holwerda B. W., 2017, *ApJ*, 837, L8
- Blázquez-Calero G., et al., 2020, *MNRAS*, 491, 1800
- Bondi H., 1952, *MNRAS*, 112, 195
- Bondi H., Hoyle F., 1944, *MNRAS*, 104, 273
- Bottrell C., et al., 2024, *MNRAS*, 527, 6506
- Bower R. G., Benson A. J., Malbon R., Helly J. C., Frenk C. S., Baugh C. M., Cole S., Lacey C. G., 2006, *MNRAS*, 370, 645
- Davies J. J., Crain R. A., Oppenheimer B. D., Schaye J., 2020, *MNRAS*, 491, 4462
- Davis M., Efstathiou G., Frenk C. S., White S. D. M., 1985, *ApJ*, 292, 371
- Dehnen W., Sempczuk M., Schönrich R., 2023, *MNRAS*, 518, 2712
- Donnari M., et al., 2019, *MNRAS*, 485, 4817
- Dubinski J., Berentzen I., Shlosman I., 2009, *ApJ*, 697, 293
- Dubois Y., Gavazzi R., Peirani S., Silk J., 2013, *MNRAS*, 433, 3297
- Erwin P., 2018, *MNRAS*, 474, 5372
- Fanali R., Dotti M., Fiacconi D., Haardt F., 2015, *MNRAS*, 454, 3641
- Fragkoudi F., Grand R., Pakmor R., Gómez F., Marinacci F., Springel V., 2024, *arXiv e-prints*, p. [arXiv:2406.09453](https://arxiv.org/abs/2406.09453)
- Fraser-McKelvie A., et al., 2020, *MNRAS*, 495, 4158
- Frosst M., Obreschkow D., Ludlow A. D., 2024, *arXiv e-prints*, p. [arXiv:2408.03375](https://arxiv.org/abs/2408.03375)
- Gargiulo I. D., et al., 2022, *MNRAS*, 512, 2537
- Garland I. L., et al., 2024, *arXiv e-prints*, p. [arXiv:2406.20096](https://arxiv.org/abs/2406.20096)
- Gavazzi G., et al., 2015, *A&A*, 580, A116
- Genel S., Vogelsberger M., Nelson D., Sijacki D., Springel V., Hernquist L., 2013, *MNRAS*, 435, 1426
- Genel S., et al., 2014, *MNRAS*, 445, 175

- George K., Joseph P., Mondal C., Subramanian S., Subramaniam A., Paul K. T., 2019, *A&A*, 621, L4
- Goulding A. D., et al., 2017, *ApJ*, 843, 135
- Harris C. R., et al., 2020, *Nature*, 585, 357
- Hohl F., 1971, *ApJ*, 168, 343
- Hoyle F., Lyttleton R. A., 1939, *Proceedings of the Cambridge Philosophical Society*, 35, 405
- Hunter J. D., 2007, *Computing in Science and Engineering*, 9, 90
- Irodotou D., et al., 2022, *MNRAS*, 513, 3768
- Jogee S., 2006, in Alloin D., ed., , Vol. 693, *Physics of Active Galactic Nuclei at all Scales*. p. 143, doi:10.1007/3-540-34621-X_6
- Kauffmann G., et al., 2003, *MNRAS*, 341, 54
- Khoperskov S., Haywood M., Di Matteo P., Lehnert M. D., Combes F., 2018, *A&A*, 609, A60
- Knapen J. H., Shlosman I., Peletier R. F., 2000, *ApJ*, 529, 93
- Kraljic K., Bournaud F., Martig M., 2012, *ApJ*, 757, 60
- Laine S., Shlosman I., Knapen J. H., Peletier R. F., 2002, *ApJ*, 567, 97
- Lee G.-H., Woo J.-H., Lee M. G., Hwang H. S., Lee J. C., Sohn J., Lee J. H., 2012, *ApJ*, 750, 141
- Li Y., et al., 2020, *ApJ*, 895, 102
- López P. D., Scannapieco C., Cora S. A., Gargiulo I. D., 2024, *MNRAS*, 529, 979
- Maciejewski W., 2004, *MNRAS*, 354, 892
- Marinacci F., et al., 2018, *MNRAS*, 480, 5113
- Masters K. L., et al., 2011, *MNRAS*, 411, 2026
- McNamara B. R., Nulsen P. E. J., 2007, *ARA&A*, 45, 117
- Melvin T., et al., 2014, *MNRAS*, 438, 2882
- Moffett A. J., et al., 2016, *MNRAS*, 457, 1308
- Murugesan C., Kilborn V., Obreschkow D., Glazebrook K., Lutz K., Džudžar R., Dénes H., 2019, *MNRAS*, 483, 2398
- Naiman J. P., et al., 2018, *MNRAS*, 477, 1206
- Nair P. B., Abraham R. G., 2010, *ApJ*, 714, L260
- Nelson D., et al., 2018, *MNRAS*, 475, 624
- Nelson D., et al., 2019a, *Computational Astrophysics and Cosmology*, 6, 2
- Nelson D., et al., 2019b, *MNRAS*, 490, 3234
- Newnham L., Hess K. M., Masters K. L., Kruk S., Penny S. J., Lingard T., Smethurst R. J., 2020, *MNRAS*, 492, 4697
- Ostriker J. P., Peebles P. J. E., 1973, *ApJ*, 186, 467
- Pillepich A., et al., 2018a, *MNRAS*, 473, 4077
- Pillepich A., et al., 2018b, *MNRAS*, 475, 648
- Pillepich A., et al., 2019, *MNRAS*, 490, 3196
- Pillepich A., Nelson D., Truong N., Weinberger R., Martin-Navarro I., Springel V., Faber S. M., Hernquist L., 2021, *MNRAS*, 508, 4667
- Pillepich A., et al., 2023, *arXiv e-prints*, p. arXiv:2303.16217
- Planck Collaboration et al., 2016, *A&A*, 594, A13
- Ramesh R., Nelson D., Pillepich A., 2023, *MNRAS*, 518, 5754
- Rodríguez-Gomez V., et al., 2015, *MNRAS*, 449, 49
- Rosas-Guevara Y., et al., 2020, *MNRAS*, 491, 2547
- Rosas-Guevara Y., et al., 2022, *MNRAS*, 512, 5339
- Sampaio V. M., Aragón-Salamanca A., Merrifield M. R., de Carvalho R. R., Zhou S., Ferreras I., 2023, *MNRAS*, 524, 5327
- Semczuk M., Dehnen W., Schönrich R., Athanassoula E., 2024, *Pattern speed evolution of barred galaxies in TNG50 (arXiv:2407.11154)*, <https://arxiv.org/abs/2407.11154>
- Sheth K., et al., 2008, *ApJ*, 675, 1141
- Sheth K., Melbourne J., Elmegreen D. M., Elmegreen B. G., Athanassoula E., Abraham R. G., Weiner B. J., 2012, *ApJ*, 758, 136
- Silva-Lima L. A., Martins L. P., Coelho P. R. T., Gadotti D. A., 2022, *A&A*, 661, A105
- Sotillo-Ramos D., et al., 2022, *MNRAS*, 516, 5404
- Springel V., 2010, *MNRAS*, 401, 791
- Springel V., White S. D. M., Tormen G., Kauffmann G., 2001, *MNRAS*, 328, 726
- Springel V., Di Matteo T., Hernquist L., 2005, *MNRAS*, 361, 776
- Springel V., et al., 2018, *MNRAS*, 475, 676
- Terrazas B. A., et al., 2020, *MNRAS*, 493, 1888
- Virtanen P., et al., 2020, *Nature Methods*, 17, 261
- Weinberger R., et al., 2017, *MNRAS*, 465, 3291
- Weinberger R., et al., 2018, *MNRAS*, 479, 4056
- Wellons S., et al., 2023, *MNRAS*, 520, 5394
- Yuan F., Narayan R., 2014, *ARA&A*, 52, 529
- Zana T., Capelo P. R., Dotti M., Mayer L., Lupi A., Haardt F., Bonoli S., Shen S., 2019, *MNRAS*, 488, 1864
- Zee W.-B. G., Paudel S., Moon J.-S., Yoon S.-J., 2023, *ApJ*, 949, 91
- Zhou Z.-B., Zhu W., Wang Y., Feng L.-L., 2020, *ApJ*, 895, 92
- Zhu L., et al., 2020, *MNRAS*, 496, 1579
- Zinger E., et al., 2020, *MNRAS*, 499, 768

This paper has been typeset from a $\text{\TeX}/\text{\LaTeX}$ file prepared by the author.